Optical transitions in strained Ge/Si superlattices

U. Schmid, J. Humlíček,* F. Lukeš,* and M. Cardona
Max-Planck-Institut für Festkörperforschung, Heisenbergstrasse 1, D-7000 Stuttgart 80, Germany

H. Presting, H. Kibbel, and E. Kasper
Daimler Benz Research Center Ulm, D-7900 Ulm, Germany

K. Eberl,† W. Wegscheider, and G. Abstreiter
Walter-Schottky-Institut, Technische Universität München, D-8046 Garching, Germany
(Received 25 July 1991)

Spectroscopic ellipsometry has been used to determine the dielectric functions of ultrathin Ge/Si superlattices with varying strain states and periodicity at room temperature. The E_1-like transitions could be resolved with the multiple-angle-of-incidence technique and in a thick, Ge-rich sample; they split up into various contributions and start to absorb the light at lower energies than compositionally equivalent alloys, as predicted theoretically. The E_2 transitions are shifted towards lower energies and split into a doublet. Both of its components show a shift due to the hydrostatic component of the internal strain, which is approximately half of what one would expect from the corresponding deformation potentials of the constituent bulk materials. While both transitions decrease in energy with increasing period, only the lower peak shows a variation of its amplitude and broadening with period, yielding evidence for confinement effects.

I. INTRODUCTION

During the past decade, spectroscopic ellipsometry has proved to be an efficient and versatile tool for the simultaneous determination of both the real and the imaginary part of the dielectric function $\varepsilon(\omega) = \varepsilon_1(\omega) + i\varepsilon_2(\omega)$ of Si, Ge, and most III-V bulk semiconductors[1] as well as that of Ge_xSi_{1-x} alloys.[2] More recently, complex multilayer structures, such as an ultrathin epitaxial Ge layer in bulk Si,[3] GaAs-$Al_xGa_{1-x}As$ heterostructures,[4] and GaAs/AlAs superlattices,[5] have been studied as well. For such multilayer systems, extensive computer analysis is required to model the experimental data and to extract the relevant parameters, such as the thicknesses of the layers and the dielectric function of the material to be investigated. We have used these techniques in order to resolve the dielectric function of Ge/Si strained-layer superlattices (SLS's) pseudomorphically grown on complex buffers in the energy region, where the superlattices are transparent, i.e., the penetration depth of the light exceeds the thickness of the superlattices. In higher absorption regions, the buffer is irrelevant for the analysis, and only the surface oxidation of the sample has to be taken into account.

Ge/Si SLS's offer exciting perspectives both from the technological and the physical point of view.[6,7] The large lattice mismatch of about 4% has drastic effects on the band structure and thus on the optical properties of the SLS's (Ref. 8) and can be used to "tailor" the electronic and optical properties to specific needs. This also offers the possibility of obtaining an artificial direct-band-gap material based on two constituents with indirect gaps.[9] The internal strain can be varied by growing the SLS's on different "virtual" substrates, such as Ge_xSi_{1-x} alloys on a Si(001) substrate,[10,11] or on a Ge substrate.[12] In the latter case all of the strain is confined in the Si layers, as long as the critical thickness is not exceeded. The other extreme is achieved if the elastic energy is minimized by distributing the strain equally in the Si (tensile strain) and Ge layers (compressive strain). Such "symmetrically strained" superlattices can theoretically be grown infinitely thick. In this paper we will demonstrate that the hydrostatic component of this strain results in a shift of the E_2 transitions that can be measured ellipsometrically, while the uniaxial component should effect the magnitude of the E_1 peak. If compared to the sharp E_1 peak of Ge_xSi_{1-x} alloys of the same composition, the corresponding transitions of the superlattice are spread out by ≈ 1 eV and start to absorb the light at lower energies. The tetragonal deformation also introduces an optical anisotropy for polarizations parallel and perpendicular to the main axis. This effect has been studied theoretically by means of the minimal basis orthogonalized linear combination of Gaussian orbitals (LCGO) technique[13] as well as by the *ab initio* linear-muffin-tin-orbital (LMTO) method.[8] Due to the small total thickness of the samples, it is however impossible to measure the polarization along the growth direction [001]. $(Ge)_n/(Si)_m$ SLS's with both n and m even have orthorhombic and not tetragonal symmetry.[14] For this reason their in-plane dielectric function should differ along the main axes ([110] and [1$\bar{1}$0] of the bulk). While such an anisotropy has been calculated with first-principles methods[8] and shown to be relevant only for very small n and m, we have not been able to detect it in our samples. This is because the individ-

ual periods of the SLS's can only be controlled within the precision of about 1 atomic monolayer (ML) during the growth, and cannot be kept to *exactly* their nominal values of n and m over hundreds of periods. The introduction of monatomic steps is expected to destroy this anisotropy. In addition, both interface diffusion, interface roughness, and monatomic steps on the substrate should invalidate this effect.

The critical points (CP's) of the dielectric function can be related to interband transitions at certain regions of the Brillouin zone (BZ) and thus to the electronic band structure of the materials. In the case of a strained $(Ge)_6/(Si)_4$ SLS, a detailed discussion of the origin of the experimentally observed CP's is given in Ref. 15.

In the following section, a description of the samples and the experimental technique and analysis is given. The results and discussion are given in Sec. III, with emphasis on the E_1 CP's and the pressure shifts as well as confinement effects of the E_2 transitions. Some concluding remarks end the paper in Sec. IV.

II. SAMPLES AND ELLIPSOMETRIC METHOD

The Ge/Si SLS's were grown by low-temperature molecular-beam epitaxy (MBE) at $\approx 300\,^{\circ}\mathrm{C}$–$350\,^{\circ}\mathrm{C}$ on two different substrates: the symmetrically strained SLS's were grown on Si(001) substrates with a homogeneous Ge_xSi_{1-x} buffer layer, so that both the Si and Ge layers are strained, whereas in the case of pseudomorphic growth on Ge substrates all of the strain is taken up by the Si layers. Strain-symmetrization has been achieved as described previously in Refs. 6 and 10. In some cases, the symmetrizing buffer consists of a more complicated structure than merely a Ge_xSi_{1-x} alloy buffer on the Si substrate, such as 60 nm of alloy plus 5 nm of Ge on the Si substrate as depicted in Fig. 1(a). Changes of the design of the buffer, such as the Ge content x and its thickness, allow for the variation of the lateral lattice constant and thus the distribution of the internal strain. The nominal thickness of these superlattice structures was 200 nm. Some samples had 20 nm of an alloy layer plus 1 nm of a Si cap on top of the SLS's, but the latter have been etched away chemically. Our ellipsometric analysis and thickness measurements show that up to 50 nm of the SLS structure have been etched away by that process. The structure of the symmetrically strained Ge-rich sample of 1-μm thickness and the series of $(Ge)_{3n}/(Si)_n$ samples grown on Ge substrates are shown schematically in Figs. 1(b) and 1(c), respectively.

All of the samples were rinsed with ethanol and methanol before the measurement in order to produce a clean surface. Oxide overlayers were taken into account by assuming a multiphase model in the analysis, as explained below. Some of the samples were n doped (Sb, see Ref. 16) to a degree ($\lesssim 10^{18}/\mathrm{cm}^3$), which does not significantly affect the ellipsometric spectra.[17] The strain-symmetrized samples also contain a high density of misfit dislocations (up to $10^{10}/\mathrm{cm}^2$). While such defects are known to introduce electronic states below the fundamental gap,[18] they are not expected to affect the strong absorption coefficients at higher energies which

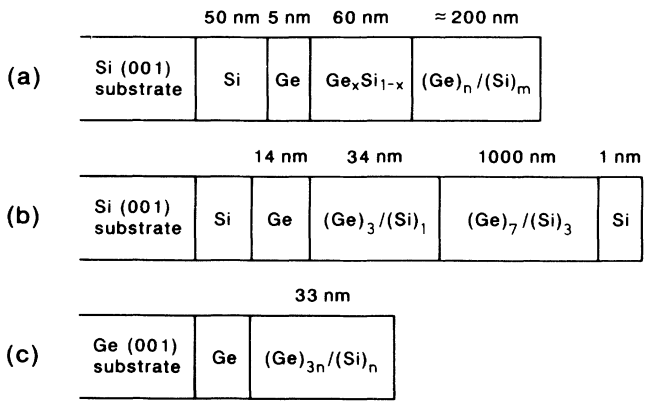

FIG. 1. Schematic structure of the samples: (a) Strain-symmetrized SLS's with n, m ranging from 2 - 12. The details of the buffer may vary in composition (x) and thickness. A series of $(Ge)_4/(Si)_6$ samples with different effective Ge content of the buffer, and thus strain contribution, has been grown this way. (b) Structure of the symmetrically strained $(Ge)_7/(Si)_3$ SLS of 1-μm thickness. (c) Series of pseudomorphically grown $(Ge)_{3n}/(Si)_n$ samples (n = 2, 3, 4) on Ge substrate.

are measured in ellipsometry.

The samples have been characterized extensively by Raman spectroscopy.[19,20] This method gives reliable values for the individual layer thicknesses due to the confinement of the optical phonons in the Ge and Si slabs as well as for the strain distribution, as explained in Ref. 20. The Raman values for the layer thicknesses are in excellent agreement (within $\approx \frac{1}{2}$ monolayer) with data obtained by profile, Rutherford backscattering, and x-ray measurements, whereas the strain values may differ by up to 30%. The Raman data, however, rely on strain shifts of three features in the Raman spectrum (the two confined modes and the Ge-Si mode) and should yield the most accurate values, at least as far as the *relative* strains are concerned.

The optical spectra were taken at room temperature in the energy range between 1.7 and 5.7 eV with a rotating analyzer spectrometer as described in Ref. 21. Ellipsometry measures the complex ratio ρ of the reflection coefficients r_p and r_s (parallel and perpendicular to the plane of incidence, respectively). This can be expressed in terms of the amplitude ratio $\tan\psi$ and the phase angle Δ:

$$\rho = \frac{r_p}{r_s} = \tan\psi e^{i\Delta} \ . \tag{1}$$

The complex dielectric function $\varepsilon(\omega) = \varepsilon_1(\omega) + i\varepsilon_2(\omega)$ can readily be derived using the two-phase model[22] (ambient and sample). While this is the "true" function for bulk material in the absence of an overlayer, it is called the "pseudodielectric" function for multilayer (including just bulk plus overlayer) systems. In such cases, the genuine values can only be obtained using multiphase models.[22] In this context, the penetration depth δ of the incident light is an important parameter:

$$\delta = \frac{\lambda}{4\pi\, n_2} \,. \tag{2}$$

Here n_2 is the extinction coefficient [$\sqrt{\varepsilon(\omega)} = n_1 + in_2$] and λ the wavelength of the light in vacuum. If the thickness of the top layer exceeds 2δ, the intensity of the light reflected from the interface below it can be neglected, as it is attenuated 50 times.[2] $\varepsilon(\omega)$ is then adequately described by a two- or three-phase model if the oxide overlayer is taken into account.

The structures observed in the $\varepsilon(\omega)$ spectra attributed to CP's can conveniently be analyzed in the second-derivative spectrum. In the case of a two-dimensional (2D) critical point, which is of importance in our analysis, its line shape can be written as[23,24]

$$\frac{d^2\varepsilon}{d\omega^2} = Ae^{i\phi}(\omega - E + i\Gamma)^{-2} \,, \tag{3}$$

where A is the amplitude, E the CP energy, and Γ the broadening parameter. The phase angle $\phi = 0, \pi/2, \pi$ corresponds to a minimum saddle point and maximum, respectively. For a discussion of other types of CP's see Ref. 24.

III. RESULTS AND DISCUSSION

A. E_1 transitions

Interference effects in Ge/Si multilayer structures have previously been shown to play an important role in ellipsometric spectra, leading to complications in interpretation.[25] Figure 2 shows the Ψ and Δ raw data (circles) of a nominal $(Ge)_4/(Si)_6$ sample, which has been designed as depicted in Fig. 1(a). The Ge content of the buffer layer amounts to $x = 0.38$. The Raman analysis yields a SLS with $n = 5.5$, $m = 6.6$, and a lateral in-plane strain of the Si layer of $\epsilon_{\parallel}^{Si} \approx 2.4\%$. We observe large oscillations in these spectra below 2.6 eV due to reflection of the incident light at the interfaces below the SLS.

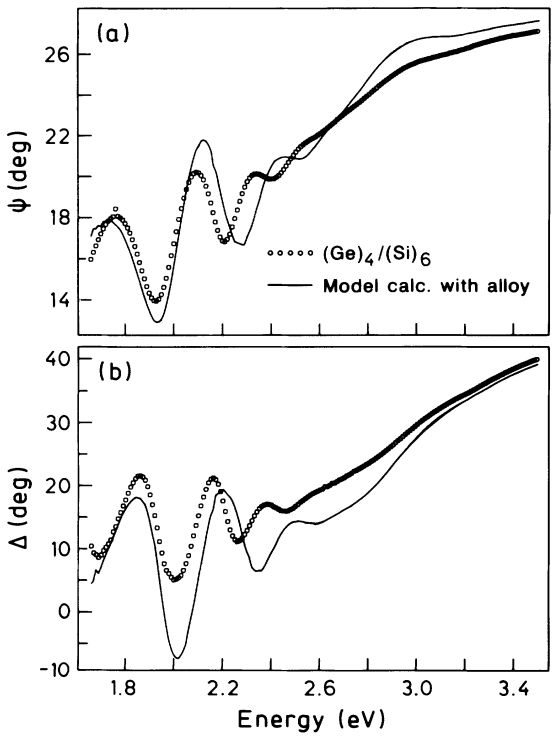

FIG. 2. Raw ellipsometric data of the nominal $(Ge)_4/(Si)_6$ SLS (circles) and model calculation (solid lines) in which the dielectric function of an unstrained $Ge_{0.4}Si_{0.6}$ alloy has been used in lieu of the SLS.

We used these regular interference patterns at the low-energy region (i.e., below 2 eV) to obtain the thickness of the SLS layers. The fit has been performed with a six-phase model, consisting of the Si substrate, four homogeneous films (including an oxide overlayer), and ambient [see Fig. 1(a)]. The thickness of the Ge film adjacent to the substrate (5 nm) and the $Ge_{0.4}Si_{0.6}$ alloy buffer (60 nm) is known from the growth conditions. Using the refractive index of the $Ge_{0.4}Si_{0.6}$ alloy for the SLS film, we have obtained a value of 150 nm for its thickness. This means that 50 nm of the SLS have been etched off.

Usually, interference patterns appear as soon as the penetration depth exceeds the thickness of the uppermost layer. Assuming that the absorption coefficient of the SLS and a $Ge_{0.4}Si_{0.6}$ alloy are comparable in this energy region, we calculate $\delta = 150$ nm at $E = 3.0$ eV, taking the alloy data from Ref. 2. The fact that the oscillations occur at lower energies is a first indication that the absorption of the SLS is somewhat higher at low energies than that of an alloy of approximately the same composition.

The results of a three-layer model, in which the dielectric functions of the SLS plus that of the 60-nm strain symmetrizing buffer have been substituted with that of a strain-free homogeneous $Ge_{0.4}Si_{0.6}$ alloy, are displayed in Fig. 2 as solid lines. In this model calculation, which is based on the Fresnel reflectance relations,[22] it is assumed that the surface terminates with a SiO_2 overlayer of 3.5 nm.

The thickness of the oxide overlayer was estimated from the high-energy ellipsometric spectra: in the region of E_2 transitions, the $\Psi - \Delta$ are almost identical to those of a semi-infinite $Ge_{0.4}Si_{0.6}$ alloy, while the values of Δ display a rigid shift proportional to the thickness of the overlayer (about 2.5°/nm). Consequently, all of the film thicknesses were kept fixed in fitting the E_1 range. We have further used tabular values of the dielectric functions of Si, Ge, $Ge_{0.4}Si_{0.6}$ alloy, and SiO_2 overlayer. The only sought parameters were the real and imaginary parts of the complex refractive index of the SLS film. We performed measurements at multiple angles of incidence ($\varphi = 60°, 65°, 70°$) in the energy region where the SLS is transparent, i.e., below 3 eV. The problem is then overdetermined (two values sought from typically three measured pairs of Ψ and Δ at three angles of incidence). The fitting procedure[26] provides a test of consistency of our model and/or experimental errors. The agreement of the best-fit and measured spectra varies within the spectral range, as expected from the wavelength-dependent experimental errors. The six-phase model was found to provide a consistent picture of the layered structure.

The result of this procedure can be viewed in the low-

energy region of Fig. 3, where we extended the data above 3 eV with the dielectric function derived from a three-phase model, i.e., SiO_2 overlayer plus SLS. In this energy range the diffraction from the lower layers can be neglected, as discussed earlier. When compared to the $\varepsilon(\omega)$ of a compositionally equivalent alloy (dashed line), we see that the absorption of the SLS is considerably stronger below $\approx$2.8 eV. This gain in oscillator strength has to be compensated for in the energy region 2.9 – 3.4 eV in order to fulfill the sum rules for $\varepsilon_2(\omega)$.[27] In contrast to the alloy, the SLS does not have a well-defined, single E_1 transition at $\approx$2.8 eV, but rather a broad band of contributions, ranging from $\approx$ 2.3 – 3.1 eV. This "multiplet" structure seems to be a fingerprint of each single Ge/Si SLS.[13] A splitting of the E_1 transitions in a $(Ge)_4/(Si)_4$ SLS into various components ranging from 2.6 – 3.2 eV has already been observed with electroreflectance,[28] while a splitting into a low, Ge-like, second extended state could be resolved by resonant Raman scattering only for larger periods ($n + m \gtrsim 20$) (Ref. 29).

The minima we found in the second derivative spectrum, $d^2\varepsilon_2/d\omega^2$, at 2.40, 2.60, 2.83, and 2.95 eV, the last being the most pronounced peak, are in excellent agreement with values theoretically predicted in Ref. 15, 2.2, 2.65, 2.9, and 3.0 eV, having corrected for the temperature shift of $\approx$ 0.1 eV. The structure around 2.6 eV should correspond to the E_0 transition. The spectrum, however, is so noisy in this region, due to the numerical uncertainties introduced in the least-squares fitting, that this agreement may be coincidental. It would thus be desirable to have a more direct evidence of the onset of absorption. For this purpose a thick sample with higher Ge content is ideal, as the E_1 band is expected to shift to lower energies with increasing Ge content, similar to the case of the alloys.[2] We thus present in Figs. 4(a) and 4(b) the real and imaginary parts of the pseudodielectric function in the two-phase model (solid lines) of a 1-μm-thick $(Ge)_7/(Si)_3$ sample [see Fig. 1(b) for its structure]. The Raman analysis fully confirms the nominal period and yields $\epsilon_{\parallel}^{Si} = 2.9\%$, which means that this sample is fully symmetrically strained. The absorption of a $Ge_{0.7}Si_{0.3}$ alloy is so strong that δ is less than the sample thickness for energies above 2.2 eV. This is also evident from a Fresnel model calculation of this structure, where $\varepsilon(\omega)$ of the alloy has been taken in lieu of that of the SLS, as depicted in Figs. 4(a) and 4(b) (dashed lines). Here, oscillations become noticeable below 2.0 eV, while $\varepsilon(\omega)$ of the $(Ge)_7/(Si)_3$ SLS remains monotonic down to the lowest energy measured (1.66 eV). This is a sign of higher absorption and demonstrates that it should be sufficient to evaluate the spectra within a three-phase model over most of the energy region (2.2 – 5.7 eV). The thick-

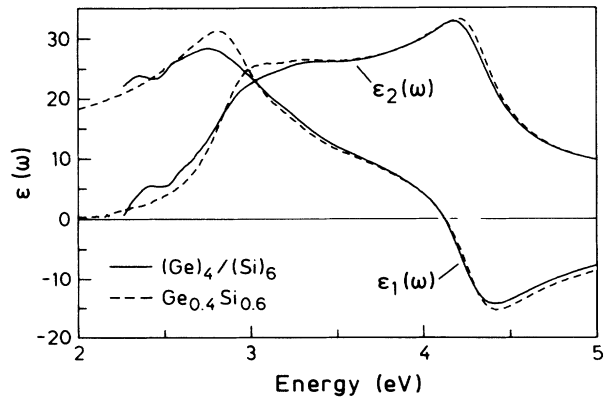

FIG. 3. Real (ε_1) and imaginary (ε_2) part of the dielectric function of the nominal $(Ge)_4/(Si)_6$ (solid lines), compared to that of $Ge_{0.4}Si_{0.6}$ alloy. Below 3 eV $\varepsilon(\omega)$ has been derived from a multiphase least-squares-fit method, using the multiple angle of incidence measurements. Above 3 eV, a three-phase model (SLS + oxide overlayer) has been used.

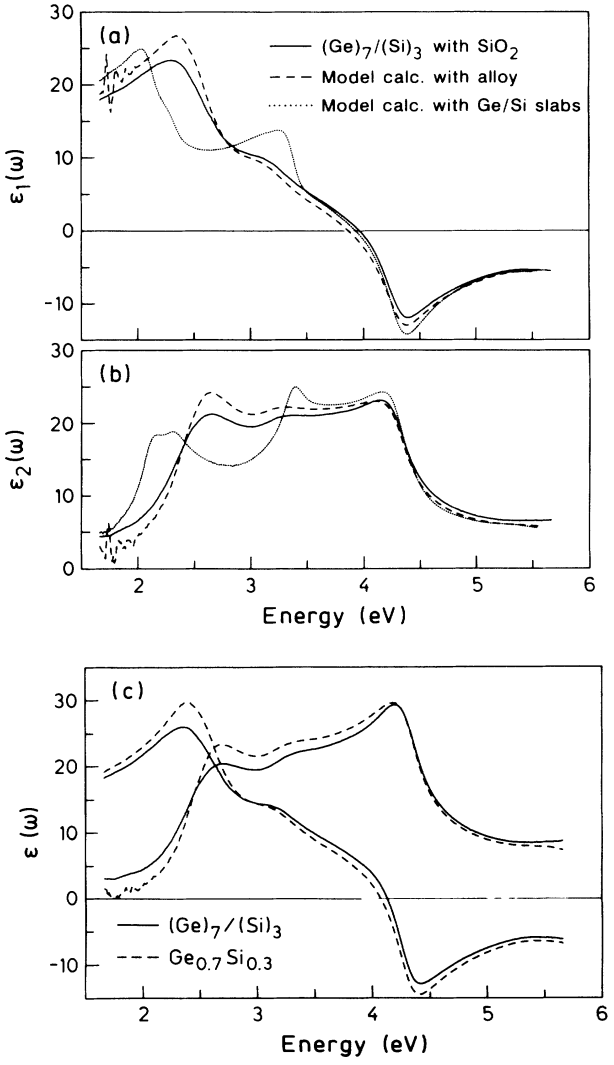

FIG. 4. Real (a) and imaginary (b) part of $\varepsilon(\omega)$ for the symmetrically strained $(Ge)_7/(Si)_3$ SLS. The solid line shows the pseudodielectric function (i.e., with oxide overlayer), and compares it to that of a model calculation where the SLS has been replaced by an unstrained $Ge_{0.7}Si_{0.3}$ alloy (dashed lines) and by a structure of 701 × (10-Å Ge/4-Å Si) (dotted line). (c) $\varepsilon(\omega)$ of the $(Ge)_7/(Si)_3$ SLS resulting from a three-phase model (solid lines), and $\varepsilon(\omega)$ of a $Ge_{0.7}Si_{0.3}$ alloy (dashed lines).

ness of the oxide overlayer is determined from the best agreement of the $\varepsilon_2(\omega)$ amplitude around the E_2 region ($\approx$4.3 eV) of the measurement and the alloy simulation, as shown in Fig. 4(b). We obtain $d(SiO_2) \approx 2.3$ nm. The measured $\varepsilon(\omega)$ shows very little structure around $E = 3.3$ eV, in contrast to what a model calculation yields if it is assumed that a 1-nm Si cap still exists, as shown in Fig. 1(b). The dominating features of thicker Si caps at this energy are also discussed in Ref. 25. If one takes into account that the fitted SiO_2 thickness amounts to $\approx$ 2.3 nm, then one can conclude that all of the Si cap layer has been oxidized, which is what we assume for the model calculations in Figs. 4(a) and 4(b). The dotted line in these figures refers to a model in which $\varepsilon(\omega)$ of the SLS has been replaced with that resulting from a sequence of (10 + 4) Å of (Ge + Si) slabs, repeated 701 times, i.e., a model based on the optical bulk properties of the constituent crystals. It is evident from Fig. 4(b) that $\varepsilon(\omega)$ of the Ge/Si SLS is neither that of the alloy nor the one resulting from a bulk model, but has its own specific properties which are somewhere between those of the two others, but rather closer to the alloy. Its "true" values as calculated from a three-phase model, i.e., without the influence of the SiO_2 overlayer, are shown in Fig. 4(c) and compared to $\varepsilon(\omega)$ of a $Ge_{0.7}Si_{0.3}$ alloy, as interpolated from the data in Ref. 2.

Here again the E_1 transitions broaden into a wide band and show a distinctive peak in $d^2\varepsilon_2(\omega)/d\omega^2$ at 2.49 eV with a weaker satellite at 2.64 eV. This is demonstrated in Fig. 5, where the second-derivative spectrum is plotted (small points), together with a fit to the critical points in the regions where this has been possible. In contrast to two weak peaks below 2.2 eV, which we believe to stem from reflection at inhomogeneities in the sample or which might still be left over from interference effects in the substrate, these pronounced peaks can be fitted well to 2D critical points, as shown in Fig. 5. The parameters of this fit are given in Table I. Both the dimension of the CP (2D) and the phase angle ϕ, which shows a mixture of a minimum and a saddle point, are in excellent agreement with those obtained for bulk Ge,[21] whereas the broadening parameters Γ are 2 – 3 times larger. The latter might easily be attributed to the imperfect structure of Ge/Si SLS's as well as to the internal strain, which splits the electronic bands in a rather entangled fashion,[15] degrading the parallelism of the valence and conduction bands involved and thus broadening the transition.

TABLE I. Values of the parameters A, E, Γ and ϕ obtained by fitting $d^2\varepsilon(\omega)/d\omega^2$ of the $(Ge)_7/(Si)_3$ SLS to a 2D CP line shape [Eq. (3)]. The results of this fit are displayed in Fig. 5.

	A (eV)	E (eV)	Γ (eV)	ϕ (deg)
E_1	5.0 (7)	2.49 (1)	0.16 (1)	78 (9)
	1.3 (5)	2.64 (1)	0.10 (1)	50 (19)
E_0'	1.3 (2)	3.19 (1)	0.13 (1)	2 (6)
E_2	7.1 (1.3)	4.21 (1)	0.16 (1)	41 (11)
	8.7 (1.2)	4.36 (1)	0.15 (1)	182 (8)

The transition at $E = 3.19$ eV is very close to the E_0' values interpolated from bulk Ge and Si ($E_0' \approx 3.17$ eV for 70% Ge contribution[21,24]). In addition, its line-shape fit yields a 2D minimum, in accordance with both Ge and Si results.[21,24] We thus have good reasons to assume that we actually observe the average E_0' transition, the

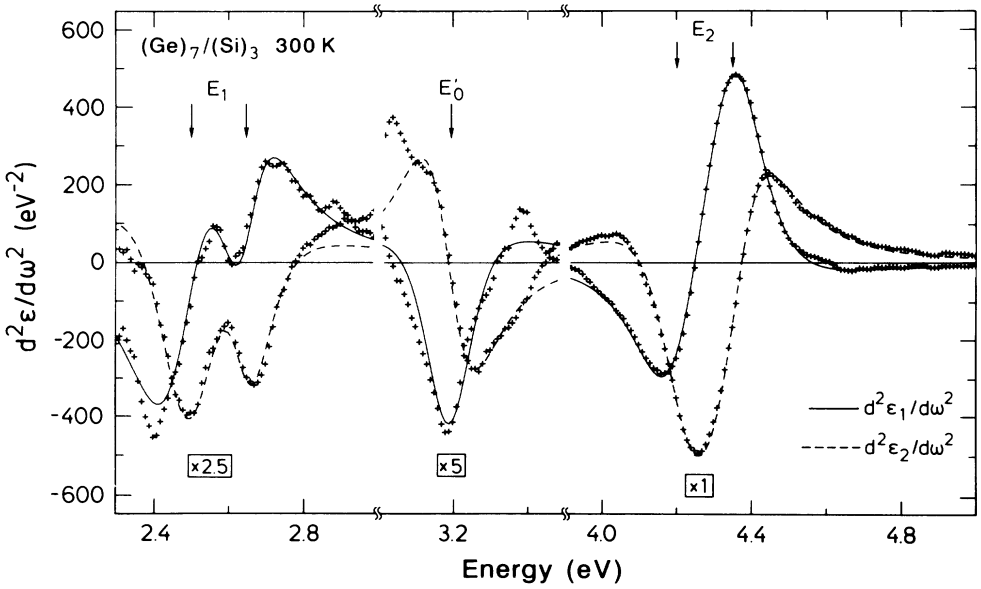

FIG. 5. Fits to the second derivatives of the real (solid line) and imaginary (dashed line) parts of the dielectric function of the strain-symmetrized $(Ge)_7/(Si)_3$ sample to 2D CP's. The readings from the vertical scale have to be divided by the factor given in the box under the various structures.

proximity of the E_0' energies of Ge and Si preventing localization, i.e., the observation of two separate values in the SLS's.

The dominant E_1 transition of the $(Ge)_7/(Si)_3$ SLS occurs at 2.49 eV, while that of the $(Ge)_4/(Si)_6$ is at 2.95. Both of these peaks do not differ too much from the E_1 transitions of alloys of the same composition, 2.46 and 2.84 eV, respectively. Shifts due to the internal strain in those SLS's should be negligible ($\lesssim 0.01$ eV), if we consider a simple linear deformation potential ansatz based on the bulk properties as discussed in Ref. 8. We thus plot in Fig. 6 the energies of the most pronounced E_1 peaks versus their Si content y, and compare them with the compositional dependence found for $Ge_{1-y}Si_y$ alloys, as described by the best-fit parabola [Eq. (4) in Ref. 2]. The open, square symbols denote the results from *ab initio* LMTO calculations,[8,15] shifted down by 0.1 eV in order to compensate for the difference in temperature (measurements at RT compared to calculations with a static lattice).[15] The two symbols at $y = 0.5$ are for the strain-symmetrized $(Ge)_5/(Si)_5$ (Ref. 30) and the $(Ge)_4/(Si)_4$ (lower value, Ref. 8), and show that this energy should not depend critically on the period $n+m$, but rather on the composition $y = m/(n+m)$ of the $(Ge)_n/(Si)_m$ SLS. We have indeed not found a large variation of the dominant E_1 transition in the experimental spectra. Figure 6 shows that the dependence of the alloy can only give a first indication of the SLS's values; the exact values differ by up to 0.17 eV, i.e., the corresponding average composition x of the SLS's can only be determined within an uncertainty of $\approx 12\%$ from the positions of the E_1 peaks. Such a large deviation is not surprising due to the complexity and splitting of the E_1 transitions in the SLS's.

Between $\approx$3.3 and 4 eV, a couple of very weak structures are observed in the $d^2\varepsilon/d\omega^2$ spectrum. It has been demonstrated[15] that they originate from zone-folded transitions, although some admixtures of reflections from inhomogeneities within the sample cannot be excluded.

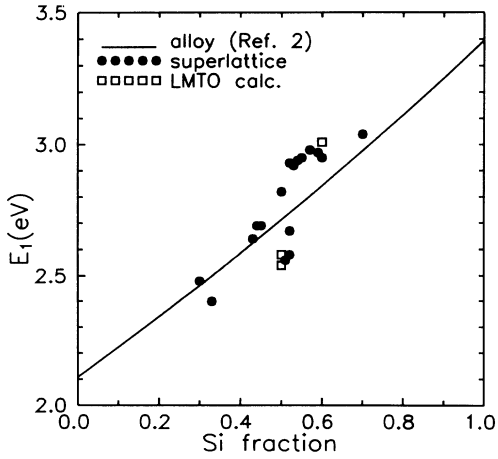

FIG. 6. Dominant E_1 peak vs Si fraction $x = m/(n+m)$ in $(Ge)_n/(Si)_m$ SLS (dots) compared to the E_1 transitions in $Ge_{1-x}Si_x$ alloys (Ref. 2). The open squares denote results from *ab initio* LMTO calculations; see text for details.

These features are so small in strength that we were not able to obtain reasonable fits to critical points.

B. E_2 transitions

The most pronounced peaks in $\varepsilon_2(\omega)$ are found around 4.3 eV in analogy to the E_2 transitions of the bulk materials. While a splitting can only be observed in the spectra only for large periods ($n+m \gtrsim 15$) at room temperature, a fit of these peaks to CP line shapes is only satisfactory when 2 CP's are considered, even for SLS's with small periods. We find that the data fit best to two 2D CP's in all cases. Whereas the phase of the lower E_2 transition (E_2^a) gives a mixture of minimum and saddle point ($40° \lesssim \phi \lesssim 60°$), the energetically higher E_2^b transition is best fitted to a mixture of a saddle point and a maximum or simply a pure maximum ($140° \lesssim \phi \lesssim 180°$), with negligible variations over the period and composition in both cases. This is similar to the E_2 gaps in the bulk materials that are also represented by a mixture of 2D minima and saddle points.[21,24] The fact that these two SLS transitions have somewhat different character is consistent with *ab initio* calculations[15] which have shown that two different, rather localized regions in the Brillouin zone ($\frac{4}{5}X$ and $\frac{4}{5}P$) contribute to these transitions. This might also explain why the amplitude A and the broadening Γ as defined in Eq. (3) show a rather different behavior when their variation with respect to the period is analyzed: whereas the measured values of A and Γ of E_2^a seem to indicate a decrease with increasing $(n+m)$, those values of E_2^b remain constant for all $(n+m)$ at approximately the values given in Table I for the $(Ge)_7/(Si)_3$ SLS. The variation with period of both A and Γ (for the E_2^a transition) is shown in Fig. 7. The large error bars for $n+m \lesssim 10$ result from a strong mixing of the two E_2 transitions for small periods. This is compatible with the fact that a splitting is visible in the spectra only for larger periods. Also, interface roughness clearly affects the magnitude of these error bars. This is evident from a comparison of the uncertainties for A and Γ of the E_2^a transition in the $(Ge)_7/(Si)_3$ SLS with excellent interface quality as given in Table I and the error bars of the other sets of samples for $n+m \approx 10$ in Fig. 7.

The energy of the E_2 transition in bulk Si (4.264 eV at $T = 300$ K, Ref. 24) is somewhat smaller than that in Ge (4.368 eV, Ref. 21) and rather close to E_2^a. As the valence band top of the Si layer is for large periods $\approx$0.5 eV below that of the Ge slab,[31] a type-II superlattice with confined conduction states in the Si layers is expected. To further examine any possible confinement effects, we plot in Fig. 8 the 2D CP energies over the Si period (E_2^a) and the Ge period (E_2^b), respectively. Three different sets of samples with comparable composition and strain are shown. Both the Si-like E_2^a and E_2^b energies decrease somewhat with increasing period. The sizeable decrease of E_2^a in the $(Ge)_{3n}/(Si)_n$ set (right panel of Fig. 8) is likely to be an artifact due to interface alloying in the extremely thin Si layer (only 2 - 4 ML). In these samples, the Ge layers are unstrained, and we have thus indicated the position of the E_2 transition of the bulk with an arrow. The E_2

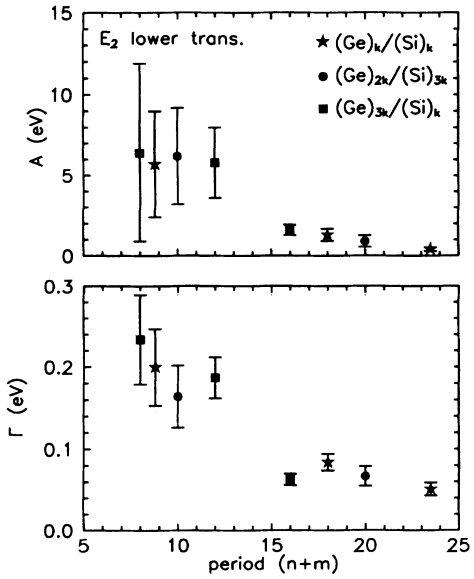

FIG. 7. Amplitude A and broadening parameters Γ as obtained from a fit to 2D CP's [Eq. (3)] of the energetically lower E_2 transitions as a function of the periodicity for three different sets of Ge/Si SLS's with different composition. In the text we interpret these data as revealing a decrease of A and Γ with increasing $(n+m)$. Data for more SLS's in the range $(12 \lesssim n+m \lesssim 16)$ are needed in order to confirm this conjecture. Note that A and Γ of the energetically higher E_2 peak remain constant.

transition of Si corrected for the shift due to the hydrostatic expansion when bulk Si is matched to the lattice constant of Ge is also drawn in that figure (E_2^{Si}/Ge). For both transitions, there is a considerable difference between the extrapolated energies $E_2^{a,b}$ for $n, m \to \infty$ and the bulk values. This is also found for the other two sets of samples presented in Fig. 8, after correction for the hydrostatic shift. The decrease in energy of both E_2^a and E_2^b when going from the left to the right section in Fig. 8 is due to the hydrostatic component of $\epsilon_{\|}^{\mathrm{Si}}$, as explained later. It seems that E_2^a is somewhat closer to the Si bulk value (within $\approx$0.05 eV) than the E_2^b transition to that of Ge.

In summary, all these experimental facts can be interpreted as sizeable confinement of the E_2^a transitions in the Si layers for large periods, and weak confinement or rather extended states for the E_2^b transitions. The "too low" lying E_2^a (compared to bulk Si) could be an indication of interface mixing, as disorder tends to lower transitions for CP's (Ref. 17). The additional drop of E_2^b is best explained by mixed states.

The strain in both slabs of the SLS's can be decomposed into a traceless uniaxial and a hydrostatic component; only the latter shifts the average energies of various indirect and direct gaps, such as E_2. The hydrostatic component, i.e., the trace of the strain tensor $\overleftrightarrow{\epsilon}$, can be expressed in terms of the lateral strain $\epsilon_{\|}$ via

$$\mathrm{Tr}\,\overleftrightarrow{\epsilon} = 2\epsilon_{\|}\left(1 - \frac{C_{12}}{C_{11}}\right), \tag{4}$$

where C_{11} and C_{12} are the elastic stiffness constants of the strained material. If we now consider the tensile and compressive strain in the Si and Ge layers, respectively, of a $(\mathrm{Ge})_n/(\mathrm{Si})_m$ SLS, and assume a linear combination of the hydrostatic shifts of those layers based on their bulk deformation potentials a_2^{Ge} and a_2^{Si}, we obtain for the resulting shift as a function of the lateral strain in the Si layer $\epsilon_{\|}^{\mathrm{Si}}$:

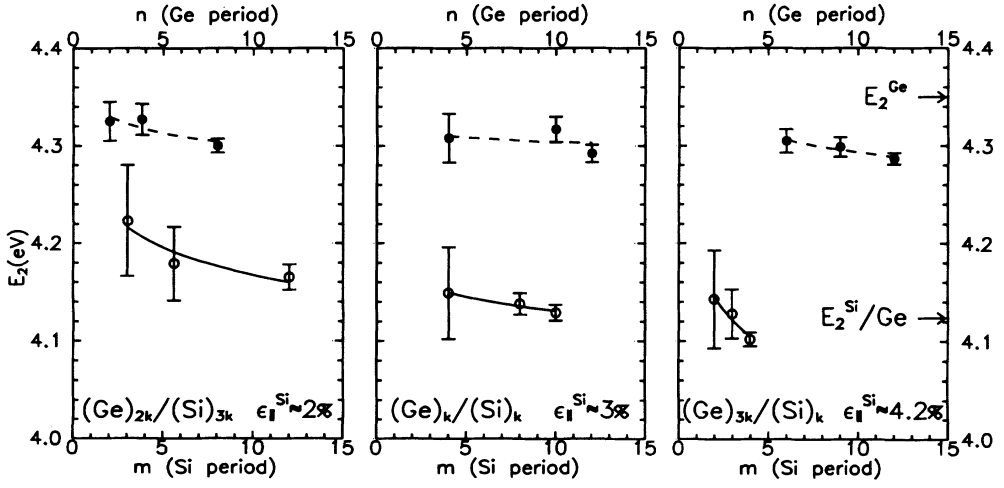

FIG. 8. Both E_2 transitions as obtained from a 2D CP line-shape fit [Eq. (3)] for three different sets of samples with *nominally* the same composition and approximately the same strain. The lower E_2^a transitions are plotted against m, and the higher E_2^b against n. The dashed and solid lines are a guide to the eye.

$$dE_2 = a_h \epsilon_{\parallel}^{\mathrm{Si}} + E_c \tag{5a}$$

with

$$a_h = 2\left[\frac{m}{n+m} a_2^{\mathrm{Si}} \left(1 - \frac{C_{12}^{\mathrm{Si}}}{C_{11}^{\mathrm{Si}}}\right) + \frac{n}{n+m} a_2^{\mathrm{Ge}} \left(1 - \frac{C_{12}^{\mathrm{Ge}}}{C_{11}^{\mathrm{Ge}}}\right)\right], \tag{5b}$$

$$E_c = \frac{2n}{n+m} a_2^{\mathrm{Ge}} \left(\frac{a_{\mathrm{Si}}}{a_{\mathrm{Ge}}} - 1\right)\left(1 - \frac{C_{12}^{\mathrm{Ge}}}{C_{11}^{\mathrm{Ge}}}\right) . \tag{5c}$$

Here, a_i are the equilibrium lattice constants of the two materials (i = Ge, Si). With the values from Ref. 32 we obtain for the "effective" hydrostatic DP $a_h \approx -4.2$ eV ($E_c \approx 0.084$ eV). We compare this DP ansatz in Fig. 9 (dashed line, with E_2 taken to be the weighted average of the bulk E_2 values) with the experimental data for a series of $(Ge)_4/(Si)_6$ SLS's (solid symbols), i.e., a well-defined set of samples with approximately the same composition and period, but only different $\epsilon_{\parallel}^{\mathrm{Si}}$. A linear fit of the data yields

$$E_2^a = \left(4.16(3) - 1.7(9)\epsilon_{\parallel}^{\mathrm{Si}} + 0.11\frac{n}{n+m}\right) \text{ eV},$$
$$E_2^b = \left(4.32(2) - 1.5(6)\epsilon_{\parallel}^{\mathrm{Si}} + 0.09\frac{n}{n+m}\right) \text{ eV} , \tag{6}$$

as indicated in Fig. 9 by the solid lines. If we fit the E_2 transition to only one CP (as we assume somewhat mixed states for $n + m \approx 10$), we obtain practically the average of the two lines drawn in this figure. The compositional dependence $cn/(n+m)$ has been calculated from the experimental data of the $(Ge)_7/(Si)_3$ SLS (open symbols in Fig. 9). Its values are in excellent agreement with the difference of the E_2 energies from bulk Ge and Si ($\Delta E_2 = c \approx 0.1$ eV). Fixing c to 0.1 eV and fitting 12 samples with $8 \lesssim n + m \lesssim 12$, but different composition, we obtain values for a_h that are somewhat higher than those given in Eq. (6), $a_h(E_2^a) = -2.3$ eV and $a_h(E_2^b) = -1.9$ eV. Owing to the large uncertainty of these values ($\lesssim 1$ eV) all we can say at this point is that the experimental DP's for both parts of the E_2 transition are approximately half of those which one would expect from a linear DP ansatz, based on the bulk properties ($a_h \approx -4.2$ eV). This is also supported by the value for a_h, which we obtain from the first-principles calculation performed on the $(Ge)_4/(Si)_4$ structure:[8] $a_h \approx -2.3$ eV, as opposed to -4.4 eV from Eq. (5b).

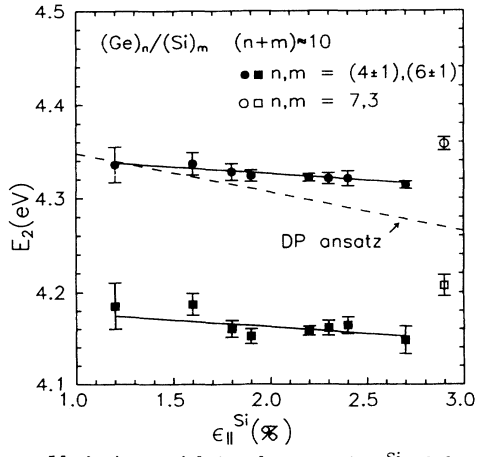

FIG. 9. Variations with in-plane strain $\epsilon_{\parallel}^{\mathrm{Si}}$ of the E_2 transitions in a series of $(Ge)_4/(Si)_6$ SLS's. The solid lines denote a linear fit to the experimental points, and the dashed line is obtained from a linear deformation potential ansatz based on bulk properties, as given in Eq. (5b). The two open symbols show experimental results from a $(Ge)_7/(Si)_3$ SLS.

IV. CONCLUSION

We have presented dielectric functions $\varepsilon(\omega)$ of strained Ge/Si SLS's, covering measurements and analysis over a three-dimensional parameter space (composition, strain, and period). These SLS's have turned out to be materials with characteristic optical properties, that can be related only in some cases to the constituting bulk materials or alloys.

The nature of the E_1 transitions has been found to be rather complicated. The large difference of those transitions in the bulk materials, in combination with strain and confinement effects, produces an intricate splitting that seems to be a "fingerprint" for each SLS. A consequence of this is the enhanced absorption in the low-energy region, where the compositionally equivalent alloys are still transparent. However, we were able to identify in the structures studied a dominant component of the E_1 transitions, from which we can estimate the composition of the SLS's with $\approx$12%.

The E_2 transitions may be easier to understand. A splitting into a doublet is observed and a quantitative description of both the shift due to the hydrostatic component of $\epsilon_{\parallel}^{\mathrm{Si}}$, as well as its compositional dependence, could be given. We have evidence for confinement effects of these states, in particular for the lower, Si-like E_2^a transitions which indicate a variation with period for their energy, amplitude, and broadening. While the period can be determined from such features in principle, more accurate data are needed in order to give a reliable quantitative description of these effects. In view of the rapid progress in the growth technology of these systems, such data should become available within the next few years.

Hopefully data will also become available for $\varepsilon(\omega)$ for polarization along the growth direction, which so far has been unmeasurable due to the small thickness of these samples ($\lesssim 1$ μm). The predicted anisotropy[8,13] is very sensitive to the strain.

ACKNOWLEDGMENTS

It is a pleasure to thank M. Garriga, S. Zollner, and M. Kelly for fruitful discussions and for providing the simulation program for our analysis. We are also indebted to U. Menczigar and R. Schorer for Raman and L. Tapfer for x-ray measurements. Parts of this work have been supported financially by ESPRIT basic research action No. 3174.

*Permanent address: Department of Solid State Physics, Faculty of Science, Masaryk University, Kotlářská, 61137 Brno, Czechoslovakia.

†Present address: Max-Planck-Institut für Festkörperforschung, Heisenbergstrasse 1, D-7000 Stuttgart 80, Germany.

[1] D.E. Aspnes and A.A. Studna, Phys. Rev. B **27**, 985 (1983).

[2] J. Humlíček, M. Garriga, M.I. Alonso, and M. Cardona, J. Appl. Phys. **65**, 2827 (1989).

[3] J.L. Freeouf, J.C. Tsang, F.K. LeGoues, and S.S. Iyer, Phys. Rev. Lett. **64**, 315 (1990).

[4] P.G. Snyder, M.C. Rost, G.H. Bu-Abbud, J.A. Wollam, and S.A. Alterovitz, J. Appl. Phys. **60**, 3293 (1986).

[5] M. Garriga, M. Cardona, N.E. Christensen, P. Lautenschlager, T. Isu, and K. Ploog, Phys. Rev. B **36**, 3254 (1987).

[6] E. Kasper, in *Strained Layer Superlattices: Materials Science and Technology*, Vol. 33 of *Semiconductors and Semimetals*, edited by T.P. Pearsall (Academic, New York, 1991), Chap. 4.

[7] T.P. Pearsall, Crit. Rev. Solid State Mater. Sci. **15**, 551 (1989).

[8] U. Schmid, N.E. Christensen, M. Alouani, and M. Cardona, Phys. Rev. B **43**, 14 597 (1991).

[9] U. Schmid, N.E. Christensen, and M. Cardona, Phys. Rev. Lett. **65**, 2610 (1990).

[10] E. Kasper, H. Kibbel, H. Jorke, H. Brugger, E. Friess, and G. Abstreiter, Phys. Rev. B **38**, 3599 (1988).

[11] The "effective" Ge content is also affected by the thickness of the alloy buffer, see Ref. 6.

[12] K. Eberl, W. Wegscheider, and G. Abstreiter, J. Cryst. Growth **111**, 882 (1991), and references cited therein.

[13] E. Ghahramani, D.J. Moss, and J.E. Sipe, Phys. Rev. B **41**, 5112 (1990); **42**, 9193(E) (1990).

[14] M.I. Alonso, M. Cardona, and G. Kanellis, Solid State Commun. **69**, 479 (1989); **70**, i(E) (1989).

[15] U. Schmid, F. Lukeš, N.E. Christensen, M. Alouani, M. Cardona, E. Kasper, H. Kibbel, and H. Presting, Phys. Rev. Lett. **65**, 1933 (1990).

[16] H. Presting, H. Kibbel, E. Kasper, and H. Jorke, J. Appl. Phys. **68**, 5653 (1990).

[17] L. Viña and M. Cardona, Phys. Rev. B **29**, 6739 (1984).

[18] For a discussion of the effects of misfit dislocations on photoluminescence measurements on Ge/Si systems, see Refs. 8 and 9, and references cited therein.

[19] M.I. Alonso, F. Cerdeira, D. Niles, M. Cardona, E. Kasper, and H. Kibbel, J. Appl. Phys. **66**, 5645 (1989).

[20] E. Friess, K. Eberl, U. Menczigar, and G. Abstreiter, Solid State Commun. **73**, 203 (1990).

[21] L. Viña, S. Logothetidis, and M. Cardona, Phys. Rev. B **30**, 1979 (1984).

[22] R.M.A. Azzam and N.M. Bashara, *Ellipsometry and Polarized Light* (North-Holland, Amsterdam, 1977).

[23] D.E. Aspnes, in *Handbook on Semiconductors*, edited by M. Balkanski (North-Holland, Amsterdam, 1980), Vol. 2, p. 109.

[24] P. Lautenschlager, M. Garriga, L. Viña, and M. Cardona, Phys. Rev. B **36**, 4821 (1987).

[25] C. Pickering, D.C. Houghton, and J.M. Baribeau, in *Proceedings of the International Conference on Modulation Spectroscopy, San Diego, 1990*, edited by F.H. Pollak, M. Cardona, and D.E. Aspnes (SPIE Proceedings, Washington, 1990), Vol. 1286, p. 163.

[26] J. Humlíček, J. Opt. Soc. Am. **2**, 713 (1985).

[27] M. Cardona, in *Optical Properties and Band Structure of Germanium and Zincblende-Type Semiconductors*, edited by E. Burstein (Academic, New York, 1972), p. 541.

[28] T.P. Pearsall, J. Bevk, J.C. Bean, J. Bonar, J.P. Mannaerts, and A. Ourmazd, Phys. Rev. B **39**, 3741 (1989).

[29] F. Cerdeira, M.I. Alonso, D. Niles, M. Garriga, M. Cardona, E. Kasper, and H. Kibbel, Phys. Rev. B **40**, 1361 (1989).

[30] U. Schmid, N.E. Christensen, and M. Cardona (unpublished).

[31] C.G. Van de Walle and R.M. Martin, Phys. Rev. B **34**, 5621 (1986).

[32] *Numerical Data and Functional Relationships in Science and Technology*, edited by O. Madelung, Landolt-Börnstein, New Series, Group III, Vol. 17a (Springer, Berlin, 1982).